J. Appl. Comput. Mech., 8(4) (2022) 1431-1444
DOI: 10.22055/jacm.2022.40173.3534

ISSN: 2383-4536
jacm.scu.ac.ir

Shahid Chamran University of Ahvaz

Journal of Applied and Computational Mechanics

Research Paper

Neural Networks with Input Dimensionality Reduction for Efficient Temperature Distribution Prediction in a Warm Stamping Process

Chun Kit Jeffery Hou[1], **Kamran Behdinan**[2]

[1] Department of Mechanical and Industrial Engineering, University of Toronto, Toronto, ON, Canada, Email: jhou@mie.utoronto.ca

[2] Department of Mechanical and Industrial Engineering, University of Toronto, Toronto, ON, Canada, Email: behdinan@mie.utoronto.ca

Received March 01 2022; Revised April 25 2022; Accepted for publication June 01 2022.
Corresponding author: C.K. Jeffery Hou (jhou@mie.utoronto.ca)

Abstract. Hot stamping involves deforming a heated blank to form components with increased mechanical strength. More recently, warm stamping procedures have been researched. The forming occurs at lower temperatures to improve process efficiency. The process is non-linear and inefficient to solve using finite element simulations and surrogate models. This paper presents the use of dimension-reduced neural networks (DR-NNs) for predicting temperature distribution in FEM warm stamping simulations. Dimensionality reduction methods transformed the input space, consisting of assembly, material, and thermal features, to a set of principal components used as input to the neural networks. The DR-NNs are compared against a standalone neural network and show improvements in terms of lower computational time, error, and prediction uncertainty.

Keywords: Machine Learning, Warm Stamping, Finite Element Analysis, Dimensionality Reduction, Artificial Neural Networks.

1. Introduction

The need for precise predictions for understanding thermal-mechanical phenomena in sheet metal workpieces is very important for reducing cost of manufacturing and waste. The components' mechanical properties strongly depend on the thermal properties throughout the process and must be accurately controlled to produce high quality products. Although much research has been conducted on the use of artificial neural networks (ANNs) for predicting and optimizing parameters in sheet metal forming simulations, issues remain with long computation times [1] and prediction uncertainty [2]. Dimensionality reduction has successfully improved surrogate model prediction accuracy and stability [3] in regression and classification tasks involving sever nonlinearities such as aerodynamics [4, 5] and calibration [6]. However, these methods have yet to be explored for sheet metal forming, where material nonlinearities are prevalent.

Sheet metal forming consists of fabrication techniques for creating automotive and aerospace components made of aluminium and steel. Among these is the hot stamping or hot deep drawing method. The metal is heated up to high temperatures in a furnace for the material to realize soak austenitisation. The blank is then quickly transitioned to the die and formed using a punch. The deformed blank is quenched in the die channel for a few seconds and released. Upon cooling, the final blank has a higher tensile strength due to the hardening that occurs during the cooling transformation. The overall hot stamping process is similar to cold stamping. However, the increased material temperature decreases flow stress and improves ductility. This has shown to improve the formability and springback control of formed components compared to cold formed results. To correctly implement the thermo-mechanics of hot forming processes, the constitutive equation for temperature-dependent material behaviour must be considered, as well as the heat transfer and friction conditions. Thus, coupled thermomechanical models are used to evaluate the material behaviour during hot stamping processes. The influence of macroparameters such as strain distributions and temperature on material properties in hot stamping has been exhaustively researched.

In the early stages of hot stamping research, experiments were conducted to understand the material and temperature requirements for hot stamping without defects. The improved hardenability and material properties from hot stamping were found to be closely related to feasible cooling rates [7], where boron composition was most influential. Naderi [8] found that only boron alloy steel grades 22MnB5, 27MnCrB5, and 37MnB4 produced fully martensitic microstructures after hot stamping. Often, sheet metal blanks are pre-coated with a protective Al-Si layer to prevent oxide scale formation with the air. The effects of this protective layer on the thermal parameters in the hot stamping process were studied by Boresetto et al. [9], while different pre-heating temperatures and sheet thicknesses for fully martensitic transformation were investigated by Lechler and Merklein [10]. They measured the phase transformations according to Vickers HV10 hardness. During the quenching phase, the blank is held at the bottom of its deformation and cooled through conduction with the tools and a full martensite microstructure is achieved. In this

Published online: June 11 2022

transformation process, the material properties and stress distribution through the blank change, which has been studied by Jing et al. [11]. The effects of cooling rate and sheet thickness were also investigated by Nakagawa et al. [12]. Their study showed that temperature drop rate increased with lower thicknesses and the consequential effects on Vickers hardness of the formed parts. The quenching time can also be reduced to improve the productivity of the hot stamping process. Nakagawa et al. [13] developed a water and die quenching process with submerged tools, where cooling the sheets with water increased heat transfer coefficient and reduced holding time by 75%. More recently, low-temperature, warm stamping methods have been explored in industry to reduce springback and improve formability of hot stamped components [14]. This process improves strain hardening, drawability, and productivity through lower cooling cycle times. After heating blanks to austenitisation temperatures, they are quickly cooled to a temperature above martensite formation before stamping to avoid bainite formation [15, 16]. Typically, the martensite forms in hot steels around 400°C [14]. Full martensite transformation is preferred, as this leads to a hot stamped steel with better tensile strength compared to partial martensite compositions. Ganapathy et al. [17] compared different hot stamping temperatures and forming speeds for producing automotive B-pillar components. They compared the low-temperature hot stamping process with the conventional hot stamping method and found that pre-cooling for stamping at lower temperatures improved productivity through reduced in-die quenching. Ganapathy et al. [18] developed another low temperature hot stamping process in martensitic 22MnB5 steel. The material was heated to a fully austenitised state at 900°C and rapid quenched to reach a fully martensitic transformation. The material was re-heated to a tempering temperature between 420-620°C and deformed. The peak stress in the blank was reduced significantly, but strain softening was prevalent. This led to reduced drawability and decreased strength, indicating this method requires further investigation to make it useful for advancing industrial manufacturing.

While experiments are useful for validation through experiments, they can be very time-consuming and inefficient for gathering large quantities of data required for extracting features in process variables. Thus, finite element models (FEMs) are commonly used for acquiring sufficient data to determine relationships between process parameters and output. As mentioned previously, the interdependence of the thermal and mechanical properties of the hot stamping process must be carefully considered in developing a numerical solution. Two methods are commonly used: sequential and fully-coupled thermo-mechanical models. Sequential solutions divide the mechanical and thermal fields into two separate problems to be solved individually. Typically, the heat transfer problem is solved first and fed as input for the stress analysis as a predefined field. Compared to fully-coupled models, sequential solutions offer the benefit of reduced computation to reach results and allows the user to specify different time-scales to solve the temperature and mechanical fields. However, for hot stamping processes, where heat is transferred between contact surfaces during deformation, a coupled thermal-displacement simulation is more appropriate. Cai et al. [19] developed a coupled thermo-mechanical FEA model for determining how process parameters influence both the structural and geometric behaviour such as cross-sectional area distortion and the temperature distribution in a local-induction-heating bending process. The authors validated the FEM with experiments and found critical bend radius increased with feed rate and the range of suitable process parameters to avoid exceeding the forming limit and minimize cross-sectional distortion. Xing et al. [20] created a FEM model for predicting springback of hot stamped parts based on experimental data of mechanics and thermal physical properties. They found that springback increased when blankholder force decreased, while springback increased with die clearance. Hajbarati and Zajkani [21] developed a novel FEM for hot stamping based on a combined Chaboche thermomechanical hardening model with anisotropy for investigating the effects of temperature variation on springback. They used an explicit Euler integration scheme to calculate stress-strain and temperature distribution throughout the hot stamping process. Liu et al. [22] developed an explicit FEM of the hot deep drawing process to investigate the effects of blankholder force and die gap on the temperature distribution of the deformed blank. Another study by Liu et al. [23] investigated the springback and temperature distribution with different austenitisation temperature and plastic properties for 22MnB5. From this study, they found that the springback was most affected by different cooling rates and nonhomogeneous shrinking of the material during the deformation.

FEMs are powerful tools for conducting parametric analyses and gathering data on experiments which would otherwise be expensive to build. However, solving nonlinear problems can become time-consuming and predictions more difficult to obtain with higher complexity models. Surrogate models such as artificial neural networks (ANNs) can remedy these computational demands and have been explored in the literature for predicting springback more quickly than FEM solutions. Dehghani and Nekahi [24] used an ANN to predict the bake hardenability and yield stress of low carbon steels in a thermomechanical model. They considered five parameters, including cooling rate, and made predictions using two hidden layers with 13 neurons. The ANN predicted the bake hardenability and final yield stress with high accuracy. Shahani et al. [2] used neural networks with FEM to predict influential parameters in a hot rolling process. The neural network was trained based on backpropagation for predicting contact stress, rolling force, and strain distribution. Although this study proved the effectiveness of ANNs to predict different thermomechanical behaviours with low average errors, the large uncertainty and variance of the prediction error was not addressed. Chokshi [25] developed an ANN for predicting phase distribution in hot stamping experiments. They found that the ANN predicted phase volume fraction with a root mean squared error of 7.7%, considering the effects of thermal history and deformation on the final microstructure. While this was an improvement on previous phase distribution prediction models, they did not investigate the coupled effects of thermal and mechanical models. Furthermore, large uncertainties in predictions were reported, indicating that further improvements to ANNs can be made to generate better predictions.

Overall, ANNs have been successful in predicting and optimizing parameters in hot stamping simulations to good accuracy. However, prediction uncertainty and model complexity due to nonlinearities remains an issue. The inclusion of nonlinear material parameters can increase dimensionality and uncertainties. This causes the number of weights in the ANN model to grow exponentially to yield accurate predictions and require more storage space to retain models which consider all the new material information.

In this work, we investigated the use of dimensionality reduction methods such as principal component analysis (PCA), partial least squares (PLS), and kernel PCA (kPCA) with neural network surrogate models for reducing computation times and uncertainty in predicting temperature distribution in a blank during a warm stamping process. The paper is organized as follows. Section 2 describes the finite element model (FEM) set-up for the warm stamping simulation test case used to evaluate the performance of our DR-NNs against standard neural networks. Next, Section 3 shows the validation of the FEM simulations with results in the literature. Section 4 provides a summary of the dimensionality reduction methods used to reduce the 54 features consisting of assembly, material, and thermal properties. This section also discusses the neural network used and concludes with a description of the general structure of the DR-NNs. Section 5 shows the prediction mean absolute error and computation time results of the DR-NNs and neural network and discusses the usefulness of dimensionality reduction for neural networks, as well as the potential for future research. Finally, Section 6 concludes the work and summarizes the key findings.

2. Finite Element Model

The warm deep drawing simulation was implemented in ABAQUS/CAE as shown in Fig. 1.

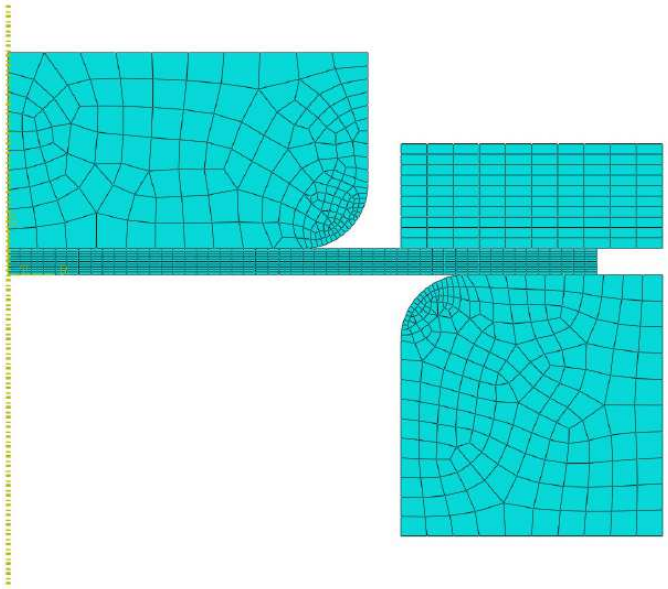

Fig. 1. 2D thermomechanical model mesh assembly of the hot deep drawing process

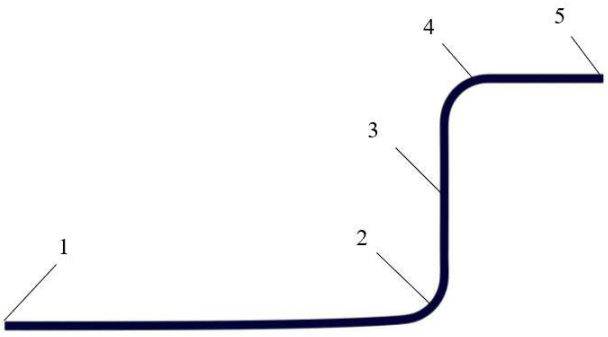

Fig. 2. Measurement points along the blank

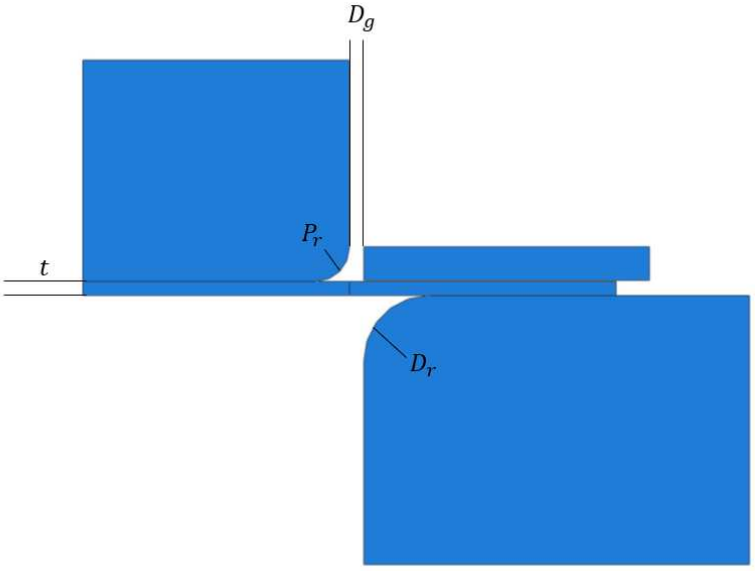

Fig. 3. Labelled assembly parameters

Table 1. Range of assembly input parameters used in the hot deep drawing simulations

Variable	Range
Initial blank temperature	450 - 650°C
Blank thickness t	1.9 – 2.1 mm
Die fillet radius D_r	9.5 – 12 mm
Quenching time	5 – 12 seconds
Cooling time	4 – 11 seconds

Table 2. Material Properties

Material Property	Tool Steel [27]	22MnB5 [28]	B1500HS [29]
Elastic Modulus [GPa]	210	210	210
Poisson's Ratio	0.3	0.3	0.37
Conductivity	24.3	40	54
Density [kg/m^3]	7800	7800	7790
Specific Heat Capacity	460	470	629

Table 3. Coefficient of Conductance (W/m^2°C) v.s Pressure for different materials

Pressure (MPa)	22MnB5 [23]	B1500HS [32]	22MnB5_US [33]
0	750	900	1300
5	1330	1500	1600
10	1750	2000	1900
20	2500	2300	2500
40	3830	3100	3700

The 2D thermomechanical model consists of a die, punch, blankholder, and blank. The assembly parts were created in an axisymmetric model space, where symmetry was defined about the x-axis and only half of the model was analyzed to reduce computation time. A coupled temperature-displacement analysis step was used for simulating the deformation of the blank under high temperature conditions. CAX4T elements were used for all parts of the assembly. A rigid constraint was defined for the tools. The mesh around the fillets of the punch and die holder were refined to improve the accuracy of the stress distribution in the blank after deformation.

The blank consisted of 900 elements with 10 elements along its thickness. A blankholder gap of 0.25 mm was imposed to prevent wrinkling and facilitate material flow into the die [26]. Under a strain rate of 0.1 s^{-1}, the sheet was deformed 35 mm. Upon reaching the end of the deformation, the deformed blank was quenched and lost heat through conduction, convection, radiation with the tools. Finally, the tools were removed, and the sheet was cooled through convection and radiation with a 25°C environment. The temperature of the sheet was measured at five different locations as shown by Fig. 2. These points were selected because the heat transfer is more critical at the centre of the sheet in contact with the punch and the areas of critical stress.

The range of assembly parameters, shown in Fig. 3, examined in this study are shown in Table 1. The ranges of values are typical values for hot stamping processes. The punch fillet radius P_r and die gap D_g were held constant at 5 mm and 0.5 mm, respectively. The microstructure of warm stamped steels fully transforms into martensite when formed at temperatures above 400°C with sufficient cooling. To facilitate martensite transformation and avoid bainite transformation, the range of initial blank temperatures during the deformation stage were kept above this value.

2.1 Material Properties

The tools used to draw the blank were assumed to be tool steel. The material properties of tool steel used in the model are shown in Table 2.

Temperature-dependent plasticity was also defined based on literature works from [19, 23, 30, 31].

2.2 Thermal Properties

The punch and sheet are in full contact along the middle of the blank during the hot deep drawing process. To accommodate for the gap between the punch and bottom of the blank in our simulation during the deformation process shown in Fig. 4, a gap conductance definition was used. Full conduction was defined between 0 to 0.3 mm clearance, as this was the measured distance between the blank and punch during the deformation phase. This was also applied to the blankholder gap as the sheet has thermal contact with the tools. The selected gap conduction method was based on the ABAQUS handbook for thermal analyses. Pressure-based conductance was also included in the simulations, shown in Table 3.

Prior to transferring the blank to the tools, air quenching was used to rapidly cool the blank to avoid banite transformation during the quenching process [12]. Different air quenched temperatures were investigated in this study. Temperature-dependent radiation and convection properties between the tools and sheet were also defined using values from [23] shown in Table 4. The radiation coefficient was converted into an equivalent convection coefficient expression for implementing into ABAQUS. These definitions were implemented as surface film conditions with a sink temperature of 25°C.

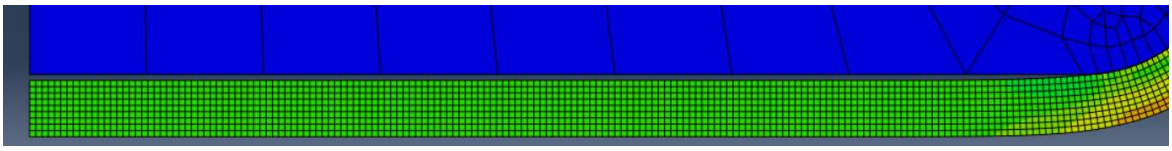

Fig. 4. Gap between punch and blank during the quenching phase

Table 4. Convection and radiation properties at tool-blank interactions for different temperatures

Coefficient of Convection (W/m^2°C)	Coefficient of Radiation (W/m^2°C)	Temperature (°C)
5.68	5.31	50
6.8	6.8	100
7.8	10.8	200
8.23	16.3	300
8.43	23.6	400
8.51	33	500
8.52	44.8	600
8.46	59.3	700

Table 5. Hot stamping input parameters; (a) Assembly parameters (b) Material parameters (c) Thermal parameters

Assembly Parameters
Die Fillet Radius
Thickness
Quench Time
Cooling Time
Temperature
Poisson's Ratio
Density

(a)

Material Parameters
Poisson's Ratio
Density
Yield (500 Degrees)
Stress at 0.1 plasticity (500 Degrees)
Stress at 0.2 plasticity (500 Degrees)
Stress at 0.3 plasticity (500 Degrees)
Stress at 0.4 plasticity (500 Degrees)
Stress at 0.5 plasticity (500 Degrees)
Stress at 0.6 plasticity (500 Degrees)
Yield (600 Degrees)
Stress at 0.1 plasticity (600 Degrees)
Stress at 0.2 plasticity (600 Degrees)
Stress at 0.3 plasticity (600 Degrees)
Stress at 0.4 plasticity (600 Degrees)
Stress at 0.5 plasticity (600 Degrees)
Stress at 0.6 plasticity (600 Degrees)
Yield (650 Degrees)
Stress at 0.1 plasticity (650 Degrees)
Stress at 0.2 plasticity (650 Degrees)
Stress at 0.3 plasticity (650 Degrees)
Stress at 0.4 plasticity (650 Degrees)
Stress at 0.5 plasticity (650 Degrees)
Stress at 0.6 plasticity (650 Degrees)
Yield (25 Degrees)
Stress at 0.1 plasticity (25 Degrees)
Stress at 0.2 plasticity (25 Degrees)
Stress at 0.3 plasticity (25 Degrees)
Stress at 0.4 plasticity (25 Degrees)
Stress at 0.5 plasticity (25 Degrees)
Stress at 0.6 plasticity (25 Degrees)

(b)

Thermal Parameters
Conductivity
Specific Heat
Convection (100 Degrees)
Convection (200 Degrees)
Convection (300 Degrees)
Convection (400 Degrees)
Convection (500 Degrees)
Convection (600 Degrees)
Convection (700 Degrees)
Radiation (100 Degrees)
Radiation (200 Degrees)
Radiation (300 Degrees)
Radiation (400 Degrees)
Radiation (500 Degrees)
Radiation (600 Degrees)
Radiation (700 Degrees)
Conduction (0 MPA)
Conduction (5 MPA)
Conduction (10 MPA)
Conduction (20 MPA)

(c)

Table 6. Properties of the validation model

Parameter	Value / Characteristic
Material	22MnB5
Punch fillet radius	5 mm
Die fillet radius	5 mm
Hot Forming Time	0.9 seconds
Quench Time	6 seconds
Cooling Time	3.8 seconds
Workpiece thickness	2 mm
Die Gap	2.05 mm
Friction Coefficient	0.1

Table 7. MAE between our FEM and [17]

Position	Measured Temperature	[23]
1	291.88	279
2	242.87	223
3	218.81	200.8
4	236.46	223.1
5	226.40	211.9

Alternatively, emissivity values can be defined for radiation heat transfer with the environment. In some experiments an emissivity of 0.6 was used 22MnBr5 and 0.5 was used for B1500HS [34]. These were converted to appropriate coefficients using Eq. (1) and fed as input to the DRNNs. Here, $T_2$and T_1 are temperatures of the two surfaces, ε is the emissivity, and σ is the Stefan-Bolzmann constant.

$$h_{eq} = \frac{\sigma\varepsilon(T_2^4 - T_1^4)}{T_1 - T_2} \tag{1}$$

2.3 Interaction Properties

Surface-to-surface interactions were defined between the blank, punch, blankholder, and die. At the contact surfaces, a friction penalty of 0.1 was imposed with default heat generation settings. The gap conductance definitions from the previous section were applied to each interaction.

2.4 Boundary Conditions

An amplitude table was used to control the displacement of the tools throughout the hot deep drawing process. During the deformation stage, the blankholder and die were fixed, and the punch motion was defined using a displacement boundary condition. At the end of the deformation, the punch is fixed throughout the quenching phase. Finally, the blankholder, punch, and die are removed using a displacement boundary condition to allow the blank to cool through radiation and convection with the environment.

2.5 Input parameters

The full set of input parameters is shown in Table 5. These parameters are separated into assembly, material, and thermal parameters.

3. Model Validation

The FEM model used for acquiring temperature distribution data was validated with the studies by Liu et al. [22, 23]. In these studies, a two-dimensional dynamic, explicit temperature-displacement deep drawing model was developed, consisting of an elasto-plastic workpiece, blankholder, punch, and die. A 2 mm blank was drawn with an 80 mm diameter punch at $0.1s^{-1}$ at 900°C with a predefined temperature field of 25°C applied to the other parts of the assembly. Heat loss due to convection and radiation have also been considered along with a cooling rate of 40°C/s from air quenching. The parameters of the validation model are shown in

Table 6.

Table 7 compares the validation results from with our simulation results. The temperature distribution was measured at different points along the blank as shown by Fig. 2.

Our model showed good agreement with the literature for predicting the temperature distribution in the thermo-mechanical simulation. The discrepancies can be explained by a few factors. The validation model used an explicit solution scheme compared to our implicit solution. Furthermore, the temperature discrepancy at the flanges is due to the validation model using blankholder force instead of a blankholder gap to facilitate material flow. To overcome this, our model includes gap conductance to allow heat transfer between position 1 and 2 throughout the process. Another reason for the discrepancies was that the blankholder in our work was defined as tool steel, while the material was unspecified in [17]. Different thermal properties for the blankholder, punch, and die likely caused the difference in results from position 4 to 5. Finally, the limiting drawing ratio of 22MnB5 was considered in our experiments. The length of the blank was scaled down from 430 mm to 160 mm to prevent excessive necking and fracture in the deep draw.

4. Dimensionality Reduction and Neural Network

Datasets containing of thousands of input parameters have become increasingly common in the manufacturing industry. These large datasets have features with highly nonlinear relationships between inputs and outputs and can be computationally expensive to train surrogate models. Dimensionality reduction methods reduce the input size of datasets using elimination, extraction, or selection to find intrinsic data characteristics in a lower dimension while retaining the key components in the dataset. In this

section, we introduce extraction-based dimensionality reduction methods and the neural network architectures used for predicting temperature distribution in the warm stamping simulation. Here, the DR-NNs retain components based on maximum variance.

4.1 Principal Component Analysis

Principal component analysis (PCA) is a linear dimensionality reduction method which decreases dataset feature space based on statistics and feature extraction. The method transforms the input parameters into linear combinations of independent variables based on maximum variance. These principal components formulate an eigenvalue problem for determining the number of components containing the largest portion of dataset information based on variance. The PCA procedure presented here is based on the work by Jolliffe & Cadima [35].

The algorithm generates new components as linear combinations of the original input variables. The new components are expressed as a covariance matrix where the variance of each variable is calculated by solving an eigenvalue equation in the form given by Eq. (2). Here λ is the set of k eigenvalues with corresponding eigenvectors a of the covariance matrix V.

$$Va = \lambda a \tag{2}$$

Typically, the principal components are centerd by subtracting by the mean of the dataset to improve the geometric interpretation of the PCA method. Furthermore, the dataset was normalized before formulating the covariance matrix to improve the quality of the output PCA components. Also, normalizing the input prevents features with larger magnitudes from skewing the portion of total variance in the dataset to those variables.

The proportion of total variance of each eigenvalue is given by Eq. (3), where tr(S) is the trace of the diagonal eigenvalue matrix. The proportion is computed to determine the number of principal components to retain. Typically, the number of principal components that make up 70% of the total variance is chosen. However, this is largely dependent on the dataset and regression results on the reduced dataset.

$$Variance\ of\ PCs_j = \frac{\lambda_j}{tr(\lambda)} \tag{3}$$

4.2 Kernel Principal Component Analysis

The PCA method is limited to datasets that are linearly separable, meaning the observations can be divided using linear hyperplanes. However, higher dimensional datasets often cannot be generalized with linear methods. The kernel principal component analysis (kPCA) method is a non-linear variant of PCA which overcomes the shortcomings of dimensionality reduction using linear hyperplanes. The kPCA procedure presented is based on the work by Lee et al. [36] and Kim et al. [37].

Starting with the input dataset, the kPCA procedure begins by mapping the input feature space to a higher-dimensional feature space known as the Herbert space through a non-linear kernel function. Following this, the linear PCA procedure is applied. The method for computing the covariance matrix C with kPCA uses a centred, non-linear mapping function Φ with N observations as shown in Eq. (4).

$$C^H = \frac{1}{N}\sum_{i=1}^{N} \Phi(\mathrm{x_i})\Phi(\mathrm{x_i}) \tag{4}$$

After diagonalizing the covariance matrix and rewriting the corresponding eigenvalue equation as a dot product of two functions shown in Eq. (5), the modified eigenvalue Eq. (6) can be solved using the procedure in linear PCA.

$$K_{ij} = k(x_i, x_j) = \Phi(\mathrm{x_i}) \cdot \Phi(\mathrm{x_i}) \tag{5}$$

$$N\lambda c = Kc \tag{6}$$

Here, the number of kPCA components to retain follows the same procedure as linear PCA. Based on the magnitudes of the eigenvalues, the number of retained components is determined by the proportion of variance.

Although the nonlinearity of kPCA makes it more computationally expensive to perform than linear PCA, the nonlinearities captured through the kernel transformation can ease the neural network training process on the reduced data. An ongoing challenge with this method remains in that kernel selection is a trivial task that is largely problem dependent.

4.3 Partial Least Squares

The PCA and kPCA methods introduced in the previous sections are unsupervised methods which perform dimensionality reduction using only the input features. Alternatively, there are supervised dimensionality reduction methods that measure the correlation between input and output variables. These methods, such as partial least squares (PLS), are superior to PCA for capturing information in each component [38].

The PLS method is a supervised, linear dimensionality reduction method that has been used in a variety of multivariate calibration and classification problems [39, 40]. The method transforms the input and response/output variables to a new feature space based on maximum covariance using the full dataset. By fitting multiple response variables into a single model, the PLS method is analogous to a multilayer perceptron. Here, the number of PLS components conserved is equivalent to the number of hidden layer nodes [41].

The objective of PLS is to perform dimensionality reduction through maximizing the cross covariances between input and output. Extensions of the PLS approach have been explored to overcome deficiencies such as overfitting [42]. In this study, the PLS1 approach introduced by Helland [43] was used.

The first latent component A_1 was expressed as Eq. (7) and found by maximizing the covariance between y and A_1 under the objective function w_1 given as Eq. (8). The number of PLS components to maintain can be determined based on minimum mean squared error or cross-validation [39].

$$A_1 = Xw_1 \tag{7}$$

$$w_1 = argmax\big(cov(Xw_1, y)\big) \tag{8}$$

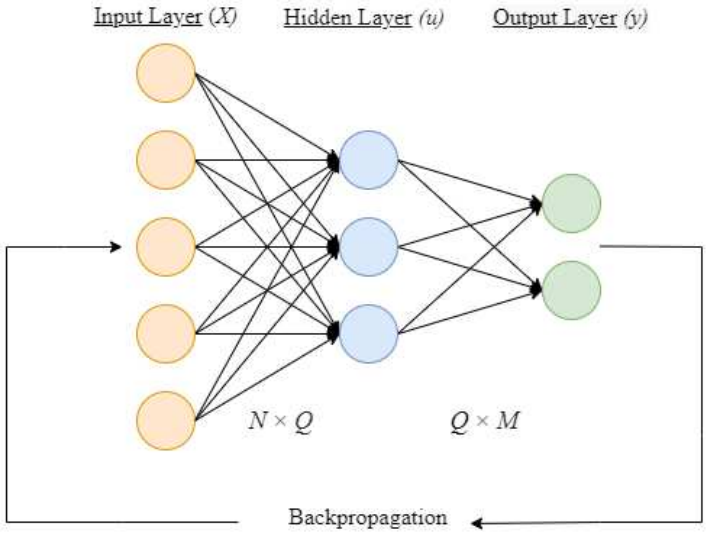

Fig. 5. Structure of an Artificial Neural Network

4.4 Artificial Neural Networks

Artificial Neural Networks (ANNs) are surrogate models based on the biological learning process of the human brain. These multi-layer algorithms are useful for high-complexity regression and non-linear classification tasks. ANNs have been popular as a supervised learning method for data-fitting, pattern recognition, and output predictions.

The mapping between input and output features are learned through training the ANNs to minimize an error function. The structure of the ANN with one hidden layer is shown in Fig. 5. ANNs contain one input and output layer with one or more hidden layers. The number of nodes in the input N and output layers M are chosen based on the number of dataset features and outputs, respectively. The number of hidden layers and hidden nodes Q were selected through trial-and-error. Careful consideration must be made as having too few hidden nodes causes the model to predict outputs with poor accuracy, while having too many nodes lead to overfitting the training data and poor generalization of unseen data. Multiple hidden layers allow the neural network to learn higher complexity mappings but requires more data and computation time. Traditionally, the structure or number of layers is chosen based on the complexity and size of the problem.

In this study, the input dataset was normalized prior to training the neural network to ease the learning process and ensure convergence of prediction error after training the model. In each sample, a normalized input feature vector x is fed into the input layer of the ANN. An activation function φ transforms the i^{th} input entry, with weights $w_{i,j}$ and biases b_j connected to the j^{th} output node of vector u, as shown in Eq. (9). Afterwards, another activation function is multiplied to the hidden layer vector values to generate the prediction vector y, shown in Eq. (10). This is repeated for subsequent samples to create a set of predictions.

$$u_j=\varphi_1\left(\sum_{i=1}^{N} w_{i,j}^1 x_i+b_j^1\right) \tag{9}$$

$$y_k=\varphi_2\left(\sum_{l=1}^{M} w_{1,k}^1 u_l+b_k^1\right) \tag{10}$$

The ReLU activation function was selected because of the reduced probability of a vanishing gradient solution. Furthermore, this piece-wise function is more computationally efficient compared to other non-linear activation functions such as sigmoid and hyperbolic tangent.

After the structure of the ANN has been determined, the model was trained by minimizing a cost function through a back-propagation optimization algorithm. During the optimization stage, the predicted outputs from the neural network are compared with the labelled ones and the weights and biases of each node are tuned to minimize the difference based on a cost function. This is known as supervised learning.

The mean absolute error (MAE) function was chosen as the cost function in this study, as shown by Eq. (11). Here, $\hat{y}$ denotes the prediction from the DR-NN and y is the labelled output.

$$MAE=\frac{1}{n}\sum_{i=1}^{n}(y-\hat{y}) \tag{11}$$

4.5 Dimensionality-Reduced Neural Network Structure

The algorithm architecture in this paper combined dimensionality reduction methods with neural networks for predicting temperature distribution in a warm stamping finite element process. PCA, PLS, and kPCA reduction-based neural networks were developed and compared with a standard neural network in terms of prediction accuracy, computation time, prediction uncertainty, and space required to store the trained model parameters.

The dataset was split into training and test sets. We further split the training data into initial training and training validation sets. The initial training dataset was used to fit the DR-NNs and the remaining validation set was used to evaluate the MAE of the model fit as the weights and biases were being updated. Finally, the test dataset was used for evaluating the performance of the fully trained DR-NNs.

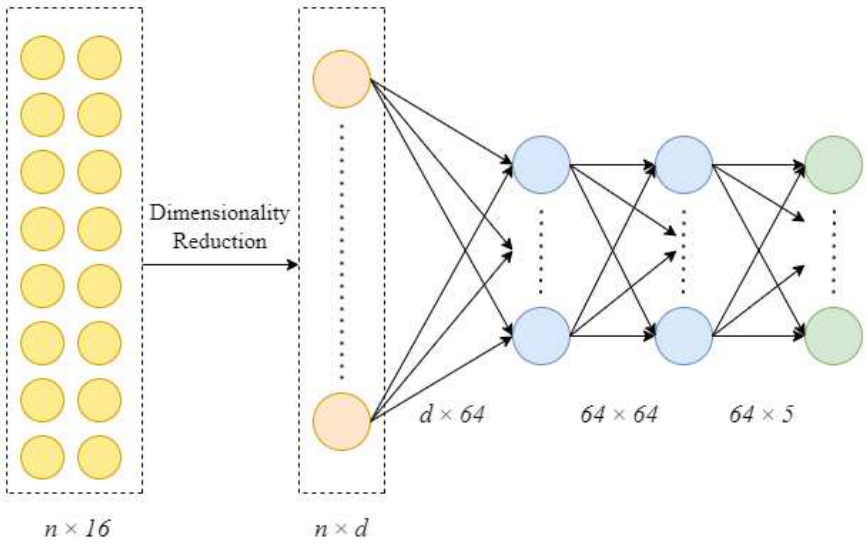

Fig. 6. DR-NN Structure. Dimensionality reduction reduces raw input to a smaller set of input nodes

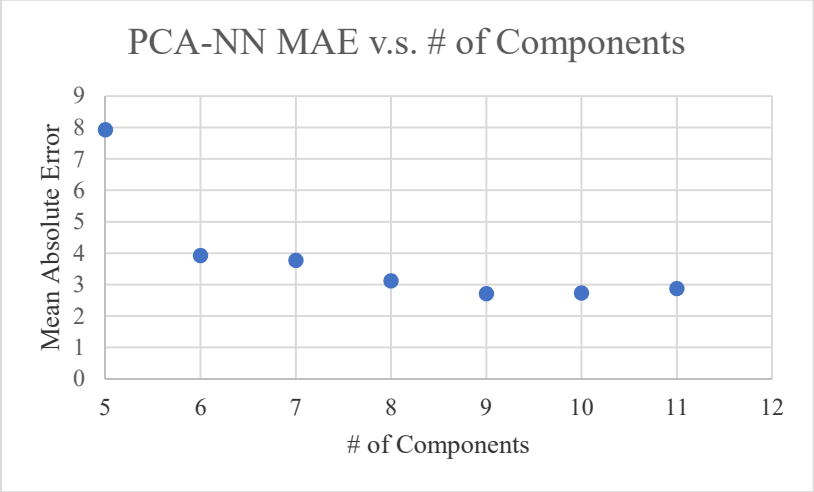

Fig. 7. PCA-NN mean absolute error v.s. # of retained Components

The structure of the DR-NNs is shown in Fig. 6. Dimensionality reduction was applied as a preprocessing step to reduce the input from 54 features to a smaller set of d features depending on the dimensionality achieved with each method. The reduced input was then fed into the two-layer, 64 node hidden layers connected to a set of output nodes representing the predicted temperature at the five measurement points. This neural network architecture was selected based on trial-and-error on the standalone neural network. A small, converging error in predictions was found with this ANN architecture, which shows that our neural network architecture is appropriate for consistently making accurate predictions. Again, the ReLU activation function was applied to each hidden layer for its good convergence behavior. For consistency, the same hidden layer structure was used in each experiment. Mini-batch Gradient Descent was selected as the optimization method for computing functional gradients to shift the prediction to a minimum mean absolute error.

5. Results and Discussion

The dimensionality-reduced neural networks (DR-NNs) were implemented in Python 3.8.10. The dimensionality reduction methods were implemented using the Scikit-learn library and the TensorFlow library was used for constructing and training the neural networks. The temperature distribution data of the warm deep drawing process was acquired using the python scripting feature in ABAQUS/CAE and observing changes in temperature at different points along the blank with the process parameters. For experimental control, only one variable was iterated in each observation. The observations were randomized and used for training the DR-NNs to avoid overfitting.

5.1 Dimensionality Selection

The number of dimensions to retain in each DR-NN was determined based on lowest validation mean absolute error (MAE) after training the models. The results for choosing the dimensionality of each DR-NN are presented in the following sections.

5.1.1 PCA-NN

Below, Fig. 7 shows the validation MAE versus the number of retained principal components in the PCA-NN after training. From observation, retaining 9 components gave a minimal prediction error. Notably, retaining more than 10 components causes overfitting in our model with the chosen hyperparameters, as shown by the increase in MAE.

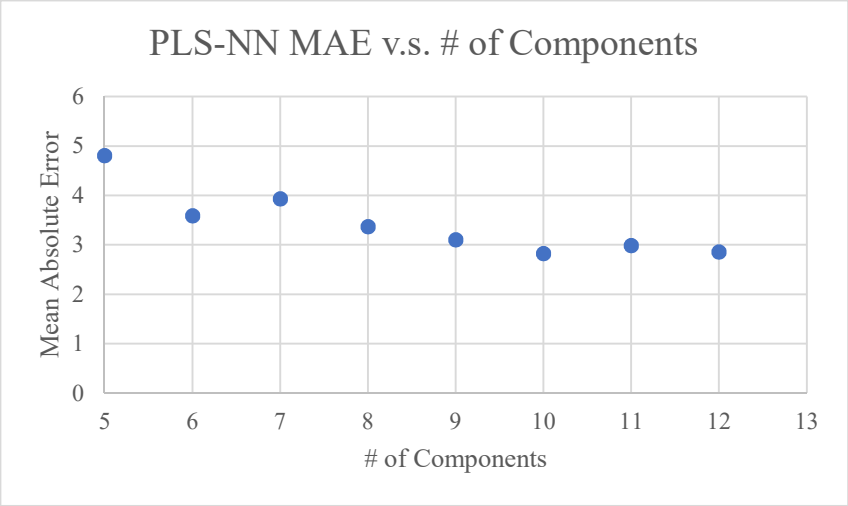

Fig. 8. PLS-NN mean absolute error v.s. # of retained components

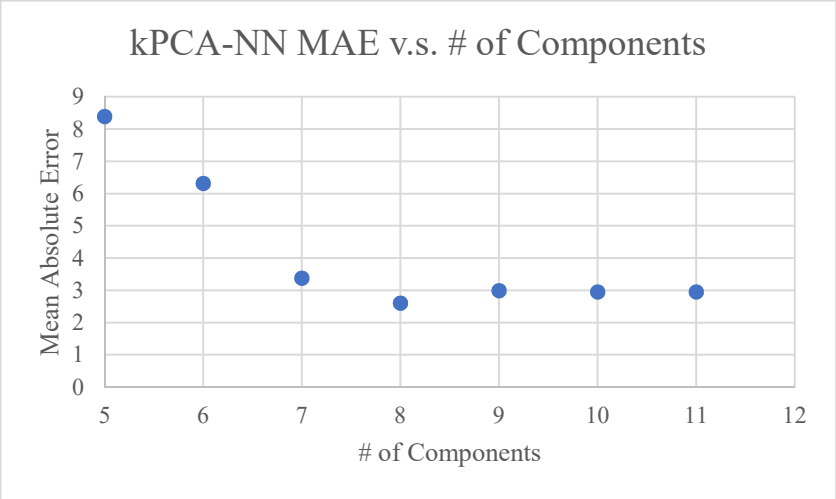

Fig. 9. Sigmoid-based kernel PCA-NN mean absolute error v.s. # of components

5.1.2 PLS-NN

The results of the average validation MAE versus the number of retained PLS components are shown in Fig. 8. Ten components were retained as the error does not decrease significantly with additional components.

5.1.3 kPCA-NN

Several kernels were evaluated for the non-linear kernel PCA dimensionality reduction. We compared the performances of radial basis functions, cosine, hyperbolic tangent, and polynomial kernels for non-linear dimensionality reduction using kPCA. Using the Scikit-learn library for kernel PCA, we implemented the kernels and combined them with a neural network for predicting the temperature distribution. Overall, the sigmoid kernel function (12) produced the lowest MAE and prediction variance. β_0 and β_1 are optimization parameters showing the MAE for each number of retained components in the sigmoid kernel-based PCA-NN. Based on the results, we chose to retain 8 kPCA components based on minimum validation MAE shown in Fig. 9.

$$k(x, y) = \tanh(\beta_0(x, y) + \beta_1) \tag{12}$$

5.2 Training Parameters and Prediction Results

The DR-NN hyperparameters were selected based on minimum validation prediction mean absolute error and uncertainty during the training phase. A total of 585 data samples were obtained and split 80-20, where 80% of the data was reserved for training and the remaining 10% was used for testing the model. The training data was further split into 90% for training and 10% for validating the prediction results after using the Adam optimizer to tune the DR-NN weights and biases based on minimum mean absolute error. A learning rate of 0.001 was used for each DR-NN model to keep a consistent comparison. At higher learning rates, the error did not converge because larger gradients caused the stochastic gradient descent to overstep the minimum error and oscillate. Table 8 summarizes the dimensionality and number of parameters trained. As shown, the number of weights and biases to be trained was significantly reduced and led to less storage space required to store the DR-NNs compared to the neural network.

A mini batch size of 32 samples was selected when performing the gradient descent to optimize DR-NN weights and biases using 500 epochs. The epochs represent the number of times the full training set was seen by the gradient descent algorithm during training.

Table 8. Dimensionality and hyperparameters for training each DR-NN model

	NN	PCA-NN	PLS-NN	kPCA-NN
Dimensionality	56	9	10	8
# of weights and biases	8246	5144	5210	5078

The DR-NNs were implemented and trained in Visual Studio Python. The computations were performed on a computer with an i7 processor with 4 cores running at 1.8 GHz on Windows 10. Below, Fig. 10 shows the training and validation MAE versus the number of epochs. The training and validation error uncertainty in the neural network was greater than the DR-NNs' as shown by the unstable behavior after training.

The DR-NNs were compared against a neural network without dimensionality reduction in terms of prediction accuracy, uncertainty, and computation time. Here, Fig. 11 and Fig. 12 show the total prediction MAE and computation times and Table 9 shows the average MAE and uncertainty of the DR-NNs and neural network averaged across 40 training runs. The results showed that applying linear and non-linear dimensionality reduction as a preprocessing step prior to training a neural network improved prediction accuracy. This is due to specific properties of the data in the original feature space being removed. The DR-NNs were trained on principal components which were not influenced by these aspects of the data. Thus, the prediction weights and biases did not divert from the global behavior of the simulation during training, resulting in lower MAE. Furthermore, the dimensionality reduction reduced the uncertainty in predictions by ignoring low-variance components which contain little or very specific information. This was also indicated by the smaller whiskers and box length in the DR-NN MAE boxplots compared to the neural network boxplot.

The performance of linear and non-linear dimensionality reduction was similar in terms of reducing computation time, prediction error, and uncertainty. This was because all the dimensionality reduction methods were able to simplify the data representation to a level where the neural network was able to predict without being influenced by noise contributed by redundant features. Although neural networks are suitable for predicting non-linear phenomena in data, the simplified structure allowed for the neural network to predict with better performance due to redundant features being removed.

A sample prediction was made using the DR-NNs and neural network shown by Table 10. The MAE was calculated using the FEM results as the baseline. From these results, the DR-NNs reduced the overall MAE in predicting the temperature distribution for a set of input parameters compared to the neural network.

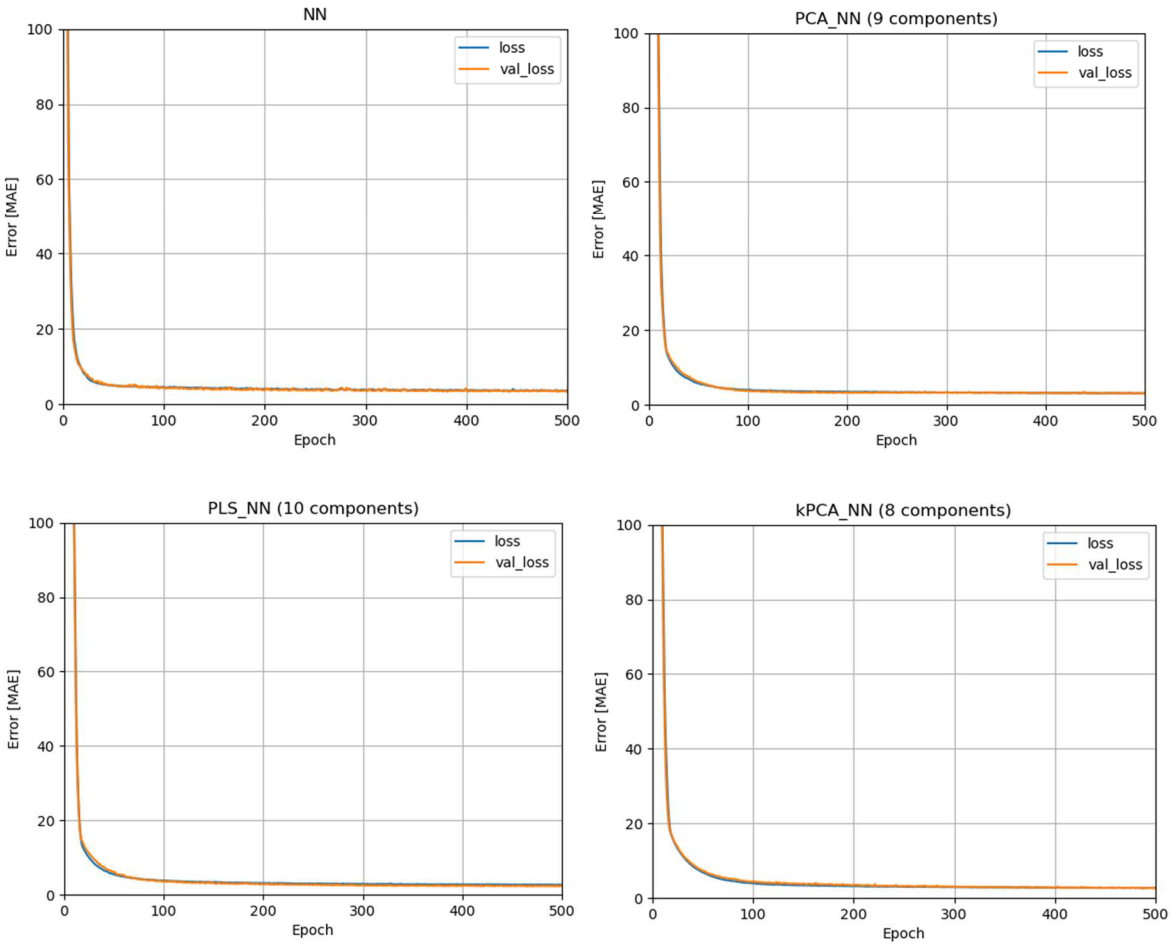

Fig. 10. Training and validation MAE of DR-NNs and neural network

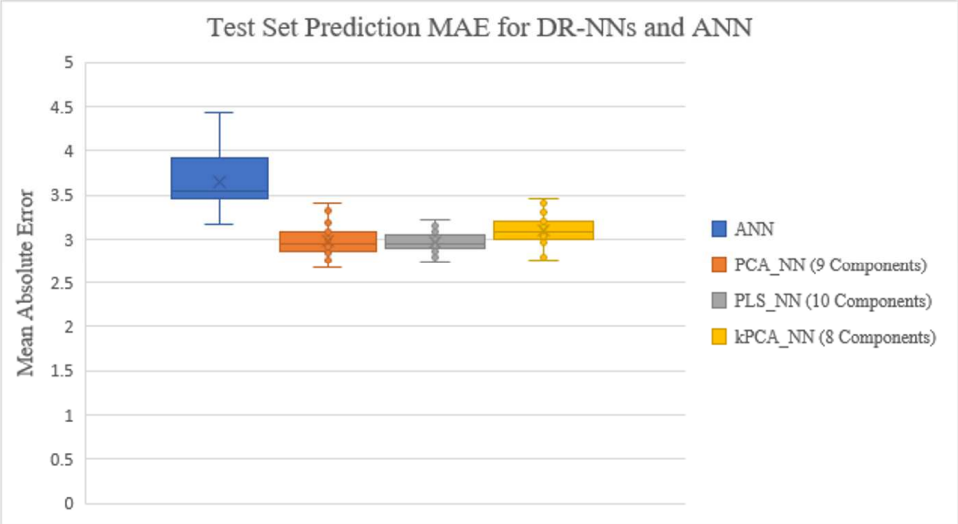

Fig. 11. MAE of temperature distribution predictions averaged across 40 training runs

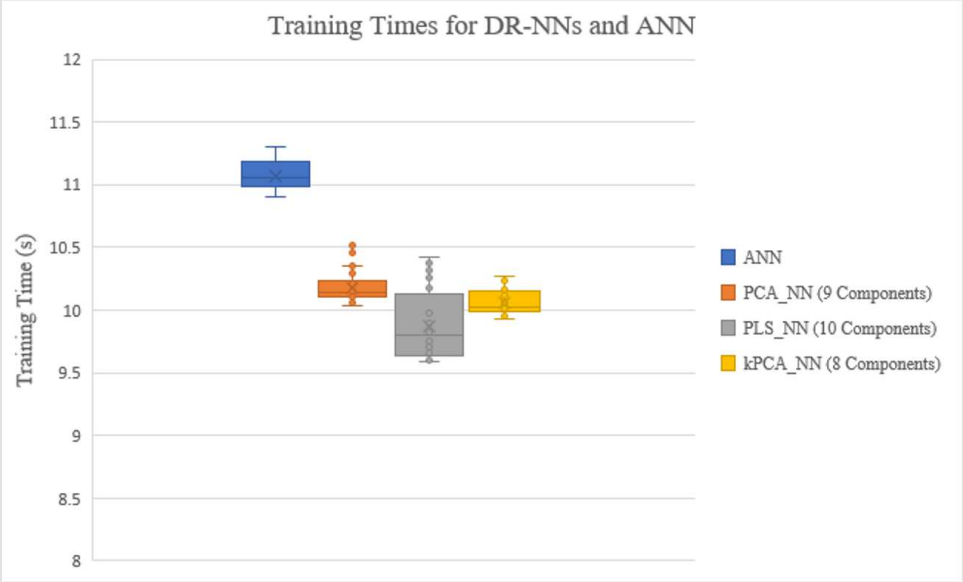

Fig. 12. Computation time in seconds for training the DR-NNs averaged across 40 training runs

Table 9. Average MAE and uncertainty when predicting the validation set

	NN	PCA_NN	PLS_NN	kPCA_NN
Average MAE	3.646	2.986	2.96	3.106
Uncertainty	0.3079	0.1682	0.1151	0.1503
Computation time (s)	11.07	10.179	9.876	10.063

Table 10. Sample prediction of temperature distribution using DR-NNs and neural network

	Point 1	Point 2	Point 3	Point 4	Point 5	Error
FEM	178.46	120.93	107.11	114.33	111.80	-
NN	179.78	121.46	108.18	114.78	112.47	0.63
PCA_NN	177.31	120.88	107.29	113.93	111.59	0.28
PLS_NN	176.84	120.33	107.11	114.01	111.89	0.35
kPCA_NN	178.71	121.33	107.80	114.30	112.18	0.30

In summary, the MAE was calculated with respect to FEM results for the temperature at the five measurement points. Each FEM simulation required three minutes to complete. Compared to this, both the DR-NNs and neural network generated accurate predictions in the order of seconds, showing the usefulness of machine learning algorithms in overcoming long computation times. The DR-NNs reduced the original 56 input feature space to a set of 8 to 10 components and lowered the average training time by 0.6 seconds and uncertainty of predictions. Furthermore, the DR-NNs showed lower prediction error uncertainty compared to the neural network. This was achieved because the DR-NNs are trained on principal components and ignoring components which contain little variance. When these components are excluded, the weights and biases in the DR-NNs are trained on only globally important information, which improves both accuracy and uncertainty of predictions.

All in all, the DR-NNs showed improvements compared to the standard neural network in terms of lower computation time, storage space required, and prediction accuracy and uncertainty. These results show the potential for DR-NNs to improve neural network training and be useful as an alternative to FEM simulations, which can require longer computation times. This can further be used in even higher dimensionality problems with input spaces in the order of thousands. The computation time in FEMs increase exponentially with complexity and DR-NNs offer a remedy to generate results in the order seconds rather than hours or days.

In future works, improvements can be made upon the neural network structure to further increase the savings on computation time, prediction uncertainty, and accuracy. In this study, we evaluated several neural network structures and selected the two-layer 64-node hidden layers based on trial-and-error. Optimization techniques can be used to identify the best DR-NN structure and learning rate. In terms of improving the FEM, temperature-dependent properties for conductivity and elastic properties may be incorporated. Furthermore, the model used in this study was limited to constant friction and die gap values. In particular, the die gap has a large influence on heat transfer in warm stamping processes and requires further research to incorporate into this study. The DR-NNs can also be used for predicting temperature change throughout the warm stamping process as well. Finally, future studies can evaluate the results of the FEM under a different range of process parameters. Overall, these improvements to the FEM can improve the quality of the data the DR-NNs are trained on.

6. Conclusions

In this paper, dimensionality reduction methods were combined with neural networks (DR-NNs) to predict temperature distribution in a warm stamping simulation. Dimensionality reduction was performed on a set of 54 input features consisting of material, assembly, and thermal parameters. The reduced components were fed into the input layer of different DR-NNs. The DR-NNs were compared against a standalone neural network and showed improvements in prediction accuracy, uncertainty, CPU space for storing model weights, and computation time. Overall, these findings prove the potential for DR-NNs to act as surrogate models to replace FEMs which can require long computation times to fully learn and predict process behavior in even higher complexity problems.

Author Contributions

The manuscript was written through the contribution of all authors. All authors discussed the results, reviewed, and approved the final version of the manuscript.

Acknowledgments

Not applicable.

Conflict of Interest

The authors declare that they have no known competing financial interests or personal relationships that could have appeared to influence the work reported in this paper.

Funding

This work was supported by the Natural Sciences and Engineering Research Council of Canada (NSERC) under grant number RGPIN-217525.

Data Availability Statements

The datasets generated and/or analyzed during the current study are available from the corresponding author on reasonable request.

References

[1] S. Kashid and S. Kumar, Applications of Artificial Neural Network to Sheet Metal Work - A Review, *American Journal of Intelligent Systems*, 2(7), 2012, 168-176.
[2] A. Shahani, S. Setayeshi, S. Nodamaie, M. Asadi and S. Rezaie, Prediction of influence parameters on the hot rolling process using finite element method and neural network, *Journal of Materials Processing Technology*, 209(4), 2009, 1920-1935.
[3] Y.-F. Zhang, P. Fitch and P. Thorburn, Predicting the Trend of Dissolved Oxygen Based onthe kPCA-RNN Model, *Water*, 12(2), 2020, 585.
[4] J. Tao, G. Sun, L. Guo and X. Wang, Application of a PCA-DBN-based surrogate model to robust aerodynamic design optimization, *Chinese Journal of Aeronautics*, 33(6), 2020, 1573-1588.
[5] D. Kapsoulis, K. Tsiakas, X. A. V. Trompoukis and K. Giannakoglou, A PCA-assisted hybrid algorithm combining EAs and adjoint methods for CFD-based optimization, *Applied Soft Computing*, 73, 2018, 520-529.
[6] M. Kamali, K. Ponnambalam and E. Soulis, Integration of surrogate optimization and PCA for calibration of hydrologic models, A WATCLASS case study, *in 2007 IEEE International Conference on Systems, Man and Cybernetics*, Montreal, Canada, 2007.
[7] P. Ravier, L. Aranda and Y. Chastel, Hot Stamping Experiment And Numerical Simulation Of Pre-coated USIBOR1500 Quenchable Steels, *in International Body Engineering Coference & Exposition*, Detroit, Michigan, USA, 1998.
[8] M. Naderi and W. Bleck, Hot Stamping of Ultra High-Strength Steels, *Materials Science*, 2008.
[9] F. Borsetto, A. Ghiotti and S. Bruschi, Investigation of the high strength steel Al-Si coating during hot stamping operations, *Key Engineering Materials*, 410, 2009, 289-296.
[10] J. Lechler and M. Merklein, Hot stamping of ultra strength steels as a key technology for lightweight construction, *Journal of Materials Science and Technology*, 3, 2008, 1698-1807.
[11] C. Jing, D. Ye, J. Zhao, T. Lin, C. Wu and Q. Lei, Effect of hot stamping and quenching & partitioning process on microstructure and mechanical properties of ultra-high strength steel, *Materials Research Express*, 8, 2021, 036506.
[12] Y. Nakagawa, T. Maeno and K.-I. Mori, Forming and quenching behaviours in hot stamping of thin quenchable sheets, *in MATEC Web of Conferences*, 2015.
[13] Y. Nakagawa, K. Mori, T. Maeno and Y. Nakao, Reduction in holding time at bottom dead centre in hot stamping by water and die quenching, *in 17th International Conference on Metal Forming*, Toyohashi, Japan, 2018.
[14] C. Tong, Q. Rong, V. Yardley, X. Li, J. Luo, G. Zhu and Z. Shi, New Developments and Future Trends in Low-Temperature Hot Stamping Technologies: A Review, *Metals*, 10(12), 2020, 1652.

[15] D. Balint, Dean TA and J. Lin, A method of forming parts from sheet steel, *US Patent 2014/0352388*, 2014.
[16] E. Ota, Y. Yogo, T. Iwata, N. Iwata, K. Ishida and K. Takeda, Formability improvement technique for heated sheet metal forming by partial cooling, *Key Engineering Materials*, 622-623, 2014, 292-283.
[17] M. Ganapathy, N. Li, M. Abspoel and D. Bhattacharjee, Experimental investigation of a new low-temperature hot stamping process for boron steels, *The International Journal of Advanced Manufacturing Technology*, 105, 2019, 669-682.
[18] M. Ganapathy, N. Li, J. Lin and D. Bhattacharjee, Investigation of a new hot stamping process with improved formability and productivity, *Precedia Engineering*, 207, 2017, 771-776.
[19] T. Cai, C. Lei, W. Yang, H. Fu and Z. Xing, Local-Induction-Heating Bending Process of B1500HS Thin-Walled Rectangular Steel Tubes: A Simulation and Experimental Investigation, *Metals*, 11(1), 2021, 132.
[20] Z. Xing, J. Bao and Y. Yang, Numerical simulation of hot stamping of quenchable boron steel, *Materials Science and Engineering A*, 499(1-2), 2009, 28-31.
[21] H. Hajbarati and A. Zajkani, A novel finite element simulation of hot stamping process of DP780 steel based on the Chaboche thermomechanically hardening model, *The International Journal of Advanced Manufacturing Technology*, 111(9-10), 2020, 1-14.
[22] H. Liu, Z. Xing, J. Bao and B. Song, Investigation of the Hot-Stamping Process for Advanced High-Strength Steel Sheet by Numerical Simulation, *Journal of Materials Engineering and Performance*, 19(3), 2010, 325-334.
[23] H. B. J. Liu, X. Zhongwen, D. Zhang, B. Song and C. Lei, Modeling and FE Simulation of Quenchable High Strength Steels Sheet Metal Hot Forming Process, *Journal of Materials Engineering and Performance*, 20(6), 2011, 894-902.
[24] K. Dehghani and A. Nekahi, Artificial neural network to predict the effect of thermomechanical treatments on bake hardenability of low carbon steels, *Materials & Design*, 31(4), 2010, 2224-2229.
[25] P. Chokshi, *Development of an artificial neural network (ANN) based phase distribution prediction model for 22MnB5 boron steel during tailored hot stamping*, PhD Thesis, University of Warwick, Warwick, 2017.
[26] H. Maan, The influence of blankholder gap on deep drawing process using finite element method, *International Journal of Mechanical Engineering and Technology*, 9(13), 2018, 1510-1518.
[27] F. Cardarelli, *Materials Handbook*, 2nd ed., London, Springer-Verlag, 2008.
[28] 22MnB5, Ovako, 17 May 2021. [Online]. Available: https://steelnavigator.ovako.com/steel-grades/22mnb5/. [Accessed 2022].
[29] H. Hou, L. Huiping and L. He, Effect of technological parameters on microstructure and accuracy of B1500HS steel parts in the hot blanking, *The International Journal of Advanced Manufacturing Technology*, 95(1-2), 2018, 3275–3287.
[30] B. Tang, F. Wu, Q. Wang, C. Li, J. Liu and G. H., Numerical and experimental study on ductile fracture of quenchable boron steels with different microstructures, *International Journal of Lightweight Materials and Manufacture*, 3, 2020, 55-65.
[31] M. Merklein, Investigation of the thermo-mechanical properties of hot stamping steels, *Journal of Materials Processing Technology*, 177(1-3), 2006, 452-455.
[32] M. Merklein, J. Lechler and T. Stoehr, Investigations on the thermal behavior of ultra high strength boron manganese steels within hot stamping, *International Journal of Material Forming*, 2(1), 2009, 259-262.
[33] J. Lechler, M. Merlein and M. Geiger, Determination of thermal and mechanical material properties of ultra-high strength steels for hot stamping, *Steel Research International*, 79(2), 2008, 98-104.
[34] A. Naganathan, *Hot Stamping of Manganese Boron Steel, Ohio*, PhD Thesis, The Ohio State University, USA, 2010.
[35] I. Jolliffe and J. Cadima, Principal component analysis: a review and recent developments, *Philosophical Transactions A*, 374, 2016, 20150202.
[36] J. Lee, C. Yoo, S. Choi, P. Vanrolleghem and I. Lee, Nonlinear process monitoring using kernel principal component analysis, *Chemical Engineering Science*, 59, 2004, 223-234.
[37] K. Kim, K. Jung and H. Kim, Face recognition using kernel principal component analysis, *IEEE Signal Processing Letters*, 9(2), 2002, 40-42.
[38] S. Maitra and J. Yan, Principle Component Analysis and Partial Least Squares: Two Dimension Reduction Techniques for Regression, 2008.
[39] H. S and B. Triggs, Feature Sets and Dimensionality Reduction for Visual Object Detection, *in British Machine Vision Conference*, Aberystwyth, 2010.
[40] S. Wold, M. Sjostrom and L. Eriksson, PLS-Regression: a basic tool of chemometrics, *Chemometrics and Intelligent Laboratory Systems*, 2001.
[41] T.C.R. Hsiao and H.K. Chiang, Partial least-squares algorithm for weights initialization of backpropagation network, *Neurocomputing*, 50, 2003, 237-247.

ORCID iD

Chun Kit Jeffery Hou https://orcid.org/0000-0003-3286-3129
Kamran Behdinan https://orcid.org/0000-0002-1873-9837

How to cite this article: Jeffery Hou C.K., Behdinan K. Neural Networks with Input Dimensionality Reduction for Efficient Temperature Distribution Prediction in a Warm Stamping Process, *J. Appl. Comput. Mech.*, 8(4), 2022, 1431–1444. https://doi.org/10.22055/jacm.2022.40173.3534